Applied Physics Letters

Exciton dynamics at a single dislocation in GaN probed by picosecond time-resolved cathodoluminescence

Cite as: Appl. Phys. Lett. **109**, 042101 (2016); https://doi.org/10.1063/1.4959832
Submitted: 07 April 2016 • Accepted: 14 July 2016 • Published Online: 26 July 2016

W. Liu, J.-F. Carlin, N. Grandjean, et al.

ARTICLES YOU MAY BE INTERESTED IN

Luminescence properties of defects in GaN
Journal of Applied Physics **97**, 061301 (2005); https://doi.org/10.1063/1.1868059

GaN surface as the source of non-radiative defects in InGaN/GaN quantum wells
Applied Physics Letters **113**, 111106 (2018); https://doi.org/10.1063/1.5048010

High spatial resolution picosecond cathodoluminescence of InGaN quantum wells
Applied Physics Letters **89**, 232109 (2006); https://doi.org/10.1063/1.2397562

© 2016 Author(s).

Exciton dynamics at a single dislocation in GaN probed by picosecond time-resolved cathodoluminescence

W. Liu,[a] J.-F. Carlin, N. Grandjean, B. Deveaud, and G. Jacopin[a]
Institute of Physics, École Polytechnique Fédérale de Lausanne (EPFL), Lausanne, Station3 CH-1015, Switzerland

(Received 7 April 2016; accepted 14 July 2016; published online 26 July 2016)

We investigate the dynamics of donor bound excitons ($D^{\circ}X_A$) at $T = 10$ K around an isolated single edge dislocation in homoepitaxial GaN, using a picosecond time-resolved cathodoluminescence (TR-CL) setup with high temporal and spatial resolutions. An $\sim$ 1.3 meV dipole-like energy shift of $D^{\circ}X_A$ is observed around the dislocation, induced by the local strain fields. By simultaneously recording the variations of both the exciton lifetime and the CL intensity across the dislocation, we directly assess the dynamics of excitons around the defect. Our observations are well reproduced by a diffusion model. It allows us to deduce an exciton diffusion length of $\sim$24 nm as well as an effective area of the dislocation with a radius of $\sim$95 nm, where the recombination can be regarded as entirely non-radiative. © *2016 Author(s). All article content, except where otherwise noted, is licensed under a Creative Commons Attribution (CC BY) license (http://creativecommons.org/licenses/by/4.0/).* [http://dx.doi.org/10.1063/1.4959832]

Blue InGaN/GaN light emitting diodes (LEDs) on sapphire (0001) substrates are currently the most efficient lighting sources for energy saving, achieving above 85% internal quantum efficiency (IQE) at low current density.[1] Indium fluctuations in the InGaN alloy have been proposed to be the main reason for such a high efficiency. The high efficiency can be achieved even with high threading dislocation density (TDD) $\sim 10^8\,\mathrm{cm}^{-2}$ in the active layers, whose non-radiative character is evidenced by cathodoluminescence (CL).[2] However, the efficiency severely drops in GaN-based LEDs with a lower indium composition, which corresponds to emission in the violet to near ultra-violet (UV) regions.[3] Violet LEDs on free standing GaN substrates ($\sim 10^6\,\mathrm{cm}^{-2}$ TDD) area provide superior color rendering index (CRI) for white lighting[4] and are a promising approach to overcome the efficiency droop.[5,6] When violet LEDs are grown on traditional sapphire substrates, the corresponding $\sim 10^8\,\mathrm{cm}^{-2}$ TDD is the main issue for achieving high efficiency. Therefore, to fully realize the potential of GaN-based LEDs emitting from violet to near UV wavelengths, it is essential to understand the carrier dynamics around dislocations.

CL is a powerful technique and widely used to study the optical properties of GaN at the nanoscale.[7–10] Since 1997, it has been confirmed, through a comparison between atomic force microscopy (AFM) and CL images, that dislocations act as non-radiative centers.[2] The non-radiative dislocations have been further identified as pure edge or mixed (edge and screw) type using a comparison between plan-view transmission electron microscopy (TEM) and CL images. An effective radius R_{eff} of the dislocation has been proposed to explain the CL efficiency around the dislocation.[11] However, the information about carrier lifetime around the dislocation, which requires simultaneous picosecond temporal and nanoscale spatial resolutions, remains difficult to access. Furthermore, the influences of R_{eff}, carrier diffusion, and the excitation volume on the CL intensity on a dislocation are still elusive.

To go beyond such limitations, picosecond time-resolved CL (TR-CL) has been proposed[12] and used to investigate the exciton diffusion in InGaN/GaN quantum well (QW), core-shell nanowires, and bulk GaN on free standing substrate.[13–15] Here, thanks to a picosecond TR-CL setup combining high temporal (<20 ps), spatial ($\sim$50 nm for the secondary electron image), and spectral ($\sim$3 meV) resolutions, we investigate the exciton dynamics at $T = 10$ K on a single dislocation in bulk GaN grown by MOVPE.[14] We obtain the distributions of emission peak energies, effective lifetimes, and CL intensities around such a dislocation. By fitting our experimental data with a simple diffusion model, we are able to define the type of dislocation and extract the R_{eff} and diffusion length of exciton. These results give precious information about the carrier dynamics around a dislocation and confirm the relevance of such a technique to elucidate the influence of dislocations on GaN-based LEDs.

The structure of the sample is the following: 2 μm GaN layer on a free standing GaN (0001) substrate with non-uniform dislocation density (ranging from $1\times10^6\,\mathrm{cm}^{-2}$ to $1\times10^7\,\mathrm{cm}^{-2}$), followed by a capping layer of 10 nm $Al_{0.05}Ga_{0.95}N$ used as a protecting layer to avoid surface recombination. In Fig. 1(a), temperature dependent photoluminescence (PL) demonstrates that donor bound exciton $D^{\circ}X_A$ (3.473 eV at 15 K) dominates the spectrum in the range of 15–50 K, whereas free exciton FX_A gradually thermally activates and only becomes predominant above 70 K.[16] The strong luminescence from $D^{\circ}X_A$ most probably comes from the high n-type doping ($\geq 2.5\times10^{18}\,\mathrm{cm}^{-3}$) inherited from the GaN substrate. Fig. 1(b) shows the CL intensity mapping of the (0001) surface of the sample in continuous excitation mode at $T = 10$ K, and the linear grayscale indicates the CL intensity. The mean electron current is around 5 nA and the acceleration voltage is 6 kV. Such an acceleration voltage has been chosen as a trade-off between the CL interaction volume

[a]Authors to whom correspondence should be addressed. Electronic addresses: we.liu@epfl.ch and gwenole.jacopin@epfl.ch

 © Author(s) 2016.

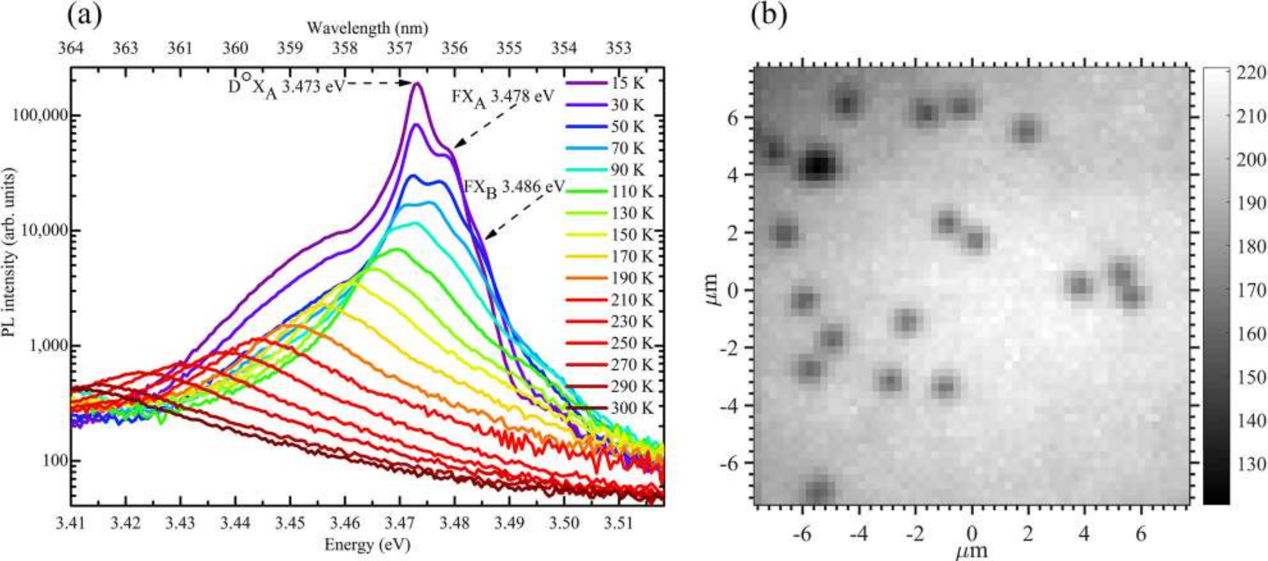

FIG. 1. (a) Temperature dependent PL from $T = 15\,\text{K}$ to $300\,\text{K}$ using a 280 nm pulsed laser at a low fluence ($\sim$1 nJ/cm^2), where the $D^{\circ}X_A$ indicates donor bound A exciton, and FX_A and FX_B are free excitons at A and B valence bands, respectively. (b) CL intensity mapping under continuous excitation mode at $T = 10\,\text{K}$, where the dark spots indicate the locations of dislocations with an areal density $\sim 8 \times 10^6\,\text{cm}^{-2}$, and the greyscale indicates the CL intensity (arb. units) in linear scale.

and the yield of CL signal when working in pulsed excitation mode. The dark spots with lower CL intensity suggest the locations of dislocations acting as non-radiative centers.[2] The average density of dislocation within this area ($\sim 240\,\mu\text{m}^2$) is $\sim 8 \times 10^6\,\text{cm}^{-2}$, which is within the order of magnitude of the dislocation density in the GaN substrate. Indeed, it has been reported that the distribution of dislocations in the GaN substrate is non-uniform.[17] In our sample, the density of dislocations revealed by the CL can be as large as $\sim 4 \times 10^7\,\text{cm}^{-2}$ in some small regions ($\sim 25\,\mu\text{m}^2$), whereas we do not observe any dislocations in some other parts of the sample.

To further understand the recombination dynamics of carriers on a single dislocation, we perform our measurements in pulsed excitation mode at 10 K. Low temperature allows us to reduce the spectral linewidth due to the suppression of phonon scattering. It is a prerequisite to precisely observe whether or not the dislocation induces a local energy gradient and to probe whether or not this gradient could affect the carrier dynamics. Fig. 2(a) presents the integrated CL intensity mapping around a dislocation at $T = 10\,\text{K}$. The blue spot in the center with $\sim$200 nm diameter shows the signature of a non-radiative dislocation. The CL intensity on the dislocation is $\sim$50% lower than that of its surroundings. Fig. 2(b) presents the corresponding mapping of the emission peak energy in the same area. The average energy all over the area is $\sim$3.473 eV, which is consistent with $D^{\circ}X_A$ emission.[16] More importantly, there is a dipole-like energy shift in the order of $\sim$1.3 meV difference around the dislocation, as illustrated by the blue and red circles. Such a dipole behavior has been observed at several dislocations under different excitation conditions in our sample. Fig. 2(c) presents the average spectra within each circle indicated in Fig. 2(b). The blue spectrum, which corresponds to the emission from the blue circle, presents a clear blue shift compared to the red spectrum from the red circle. This dipole-like energy shift clearly indicates the presence of an edge or mixed type of dislocation, which induces local strain fields.[18,19]

In Fig. 2(d), a continuum elastic model reproduces the dipole-like energy shift with the $\sim$1.3 meV difference and $\sim$400 nm separation between the two poles, which are consistent with the experimental results. In detail, supposing a pure edge dislocation with the Burgers vector $b = \frac{1}{3}\langle 11\bar{2}0\rangle$, the dipole-like energy shift ΔE_g is given by

$$\Delta E_g = (a_1 + b_1)\varepsilon_{zz} + (a_2 + b_2)(\varepsilon_{xx} + \varepsilon_{yy}), \tag{1}$$

$$\varepsilon_{xx} = \frac{b}{4\pi} y \frac{(3c_{11} + c_{12})x^2 + (c_{11} - c_{12})y^2}{c_{11}(x^2 + y^2)^2}, \tag{2}$$

$$\varepsilon_{yy} = \frac{b}{4\pi} y \frac{-(c_{11} + 3c_{12})x^2 + (c_{11} - c_{12})y^2}{c_{11}(x^2 + y^2)^2}, \tag{3}$$

where $a_{i=1,2}$ and $b_{i=1,2}$ are hydrostatic deformation potentials, $c_{ij=11,12}$ are the elastic constants of GaN, x and y indicate the location based on the Cartesian coordinate $(x \parallel \langle 11\bar{2}0\rangle$, $y \parallel \langle 1\bar{1}00\rangle$, $z \parallel \langle 0001\rangle)$, and $\varepsilon_{i=xx,yy,zz}$ are strain tensors, in which $\varepsilon_{zz} = 0$, considering the Burgers vector is parallel to the xy plane. All the above values are taken from Ref. 19. Considering the interaction volume and the diffusion of injected carriers, ΔE_g is convoluted with a two-dimensional (2D) (xy plane) Gaussian distribution with a full width at half maximum $FWHM = 220 \pm 30\,\text{nm}$, which is the only fitting parameter and determines both the energy shift and the separation distance of the dipole. Therefore, our simulation, which includes the $FWHM$ for the interaction volume, shows that the optical properties around this particular dislocation are dominated by the edge component, with $\langle\bar{1}100\rangle$ orientation, as the red mark of dislocation in Fig. 2(b) shows. In Ref. 19, the distance between the two poles was found to be $\sim 5\,\mu\text{m}$, which is one order of magnitude more than what we observe here ($\sim$400 nm). The reason behind this discrepancy is the following: the strain fields around a dislocation present a divergence exactly at the center of dislocation. As a result, the distance between the observed maximum and minimum in energy only comes from the limited spatial resolution.

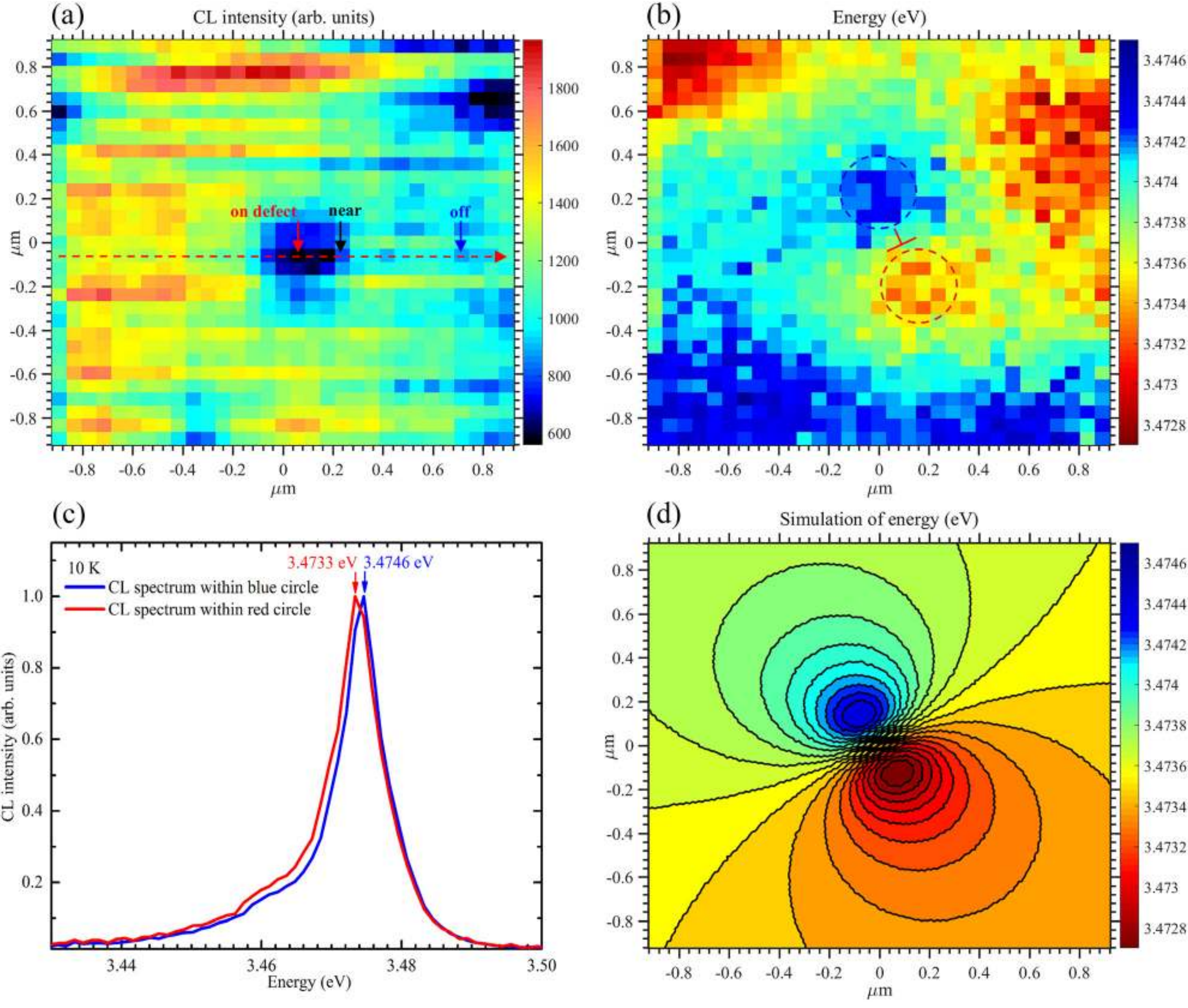

FIG. 2. (a) CL intensity mapping at $T = 10\,K$ obtained under the pulsed excitation mode of the microscope, the color bar indicates the CL intensity (arb. units) in linear scale. (b) Peak energy mapping of emission in the same area corresponding to (a). The color bar indicates the peak energy (eV) in the linear scale; the blue and red dashed circles indicate the dipole-like energy shift, in the middle of which appears a mark at the position of the dislocation. (c) Normalized CL spectra integrated over the corresponding circles (blue/red) as shown in (b). (d) Results of the simulation of the emission energy shift corresponding to (b), with the fitting parameter *FWHM* of interaction volume = 220 ± 30 nm.

Thanks to a much better spatial resolution of CL compared to micro-photoluminescence, the two peaks appear closer in our experiments, which confirms the relevance of our approach.

The above analysis is useful to determine the type of dislocation and its influence on the local bandgap; however, we do not observe any significant impact of this dipole on the carrier diffusion. Indeed, the CL intensity around the dislocation in Fig. 2(a) does not exhibit any favored direction. This could be explained by the small energy shifts induced by the dislocation (±0.7 meV), which is less than the thermal energy at $T = 10\,K$ and as such does not play a significant role on the exciton dynamics.

TR-CL is then employed to probe the exciton recombination dynamics around the dislocation. The effective lifetime τ_{eff} is measured along the red dashed arrow plotted in Fig. 2(a). Fig. 3(a) shows a streak image recorded all along the red dashed arrow in Fig. 2(a) and demonstrates that the decay time is not energy dependent in our sample. Fig. 3(b) presents the decay curves probed at different distances from the dislocation, as denoted by the solid arrows (on, near, and off the dislocation) in Fig. 2(a), and reveals two main features when closer to the dislocation: (1) The CL intensity $I_{CL}(t = 0)$ at early delay time is lower and (2) the effective lifetime τ_{eff} is shorter. In Figs. 3(c) and 3(d), more details are given by the one-dimensional (1D) mappings of $I_{CL}(t = 0)$ and τ_{eff}, extracted from a mono-exponential fit. $I_{CL}(t = 0)$ drops by 40% at the dislocation compared to the surroundings, and τ_{eff} reduces from 125 ps to 90 ps.

To explain both the spatial dependent effective lifetime τ_{eff} and the CL intensity at early delay time $I_{CL}(t = 0)$, we propose a model based on a 2D (*xy* plane) diffusion equation which considers a region around the dislocation, defined by an effective radius R_{eff}, where the recombination is treated as entirely non-radiative and instantaneous.[20] This assumption is based on the fact that, when the electron beam is located at the dislocation, a drop of intensity appears at early delays, which indicates the non-radiative processes at the dislocation are faster than our temporal resolution (<20 ps). For simplicity, we set the dislocation at the origin of the simulation area. When an exciton is outside the R_{eff} of dislocation, it can diffuse and recombine either radiatively or non-radiatively, and

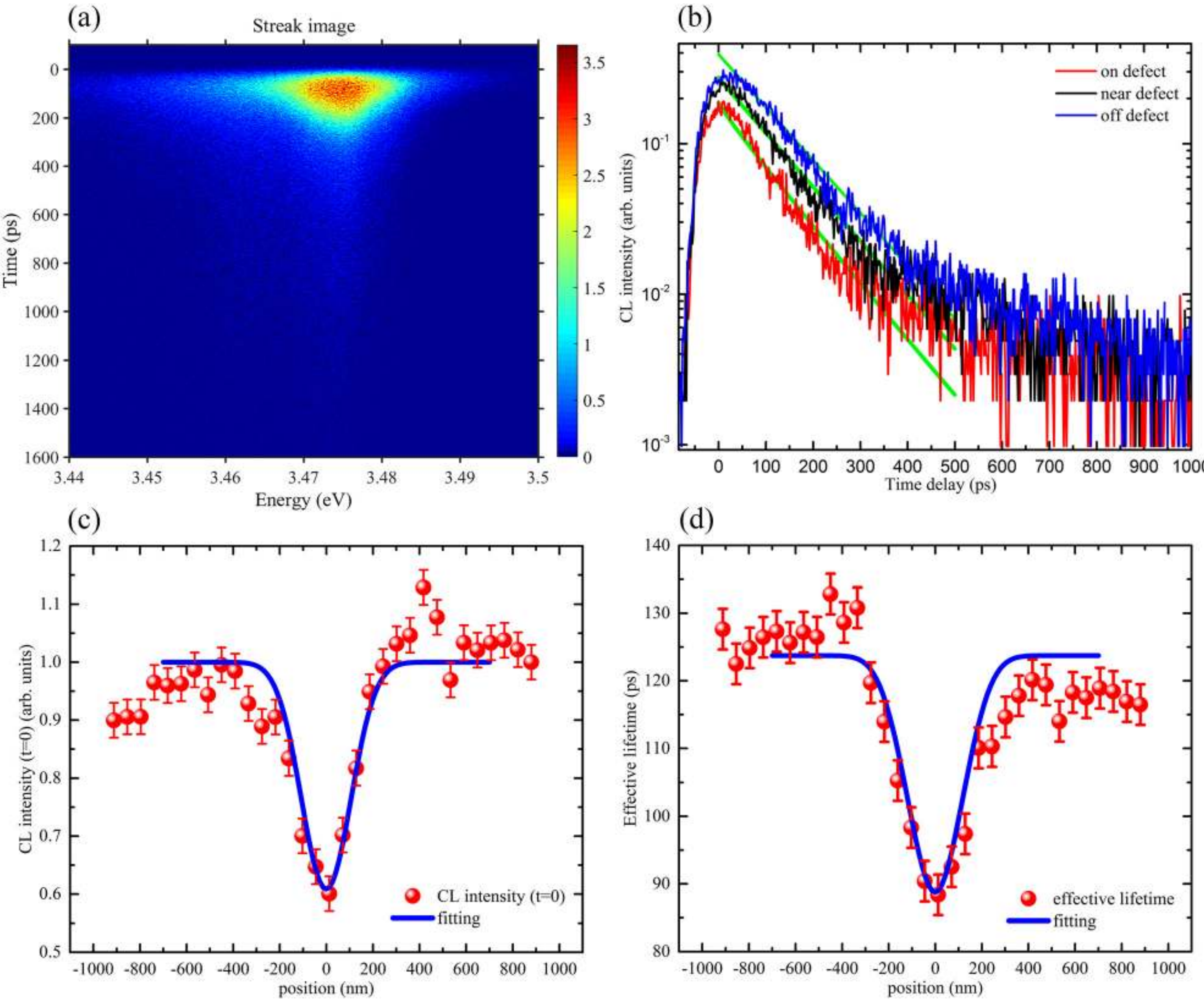

FIG. 3. (a) Integrated streak image of 1D mapping along the line illustrated by the red dashed arrow in Fig. 2(a). The color bar indicates the CL intensity (arb. units) in linear scale. (b) Decay curves measured at different distances from the dislocation, as indicated by the solid arrow lines in Fig. 2(a) (on, near, and off the dislocation), and the fitting curves (green lines) corresponding to each decay curves. (c-d) 1D mappings of normalized I_{CL} $(r_0, t=0)$ and τ_{eff} (r_0), and the best fits (blue lines) with the following parameters: diffusion coefficient $D = 4.5 \pm 0.2\,\mathrm{nm}^2/\mathrm{ps}$, effective lifetime far from the dislocation $\tau_{eff,\infty} = 125 \pm 3$ ps, effective radius of the dislocation $R_{eff} = 95 \pm 3$ nm, *FWHM* of interaction volume $= 220 \pm 4$ nm.

the density as a function of location and time can be described as below:

$$\frac{d}{dt}n(r-r_0,t) = D\nabla^2 n(r-r_0,t) - \frac{n(r-r_0,t)}{\tau_{eff,\infty}}, \quad \text{if } r > R_{eff}, \tag{4}$$

where $n(r-r_0,t)$ is the exciton density at location r and at time t diffusing from r_0 (the position of the electron beam), D is the diffusion coefficient, and $\tau_{eff,\infty}$ is an effective lifetime far from the dislocation. On the other hand, when the excitons diffuse into the effective area of dislocation, which is regarded as a *dead zone*,[11] the exciton density is forced to vanish

$$n(r-r_0,t) = 0, \quad \text{if } r < R_{eff}. \tag{5}$$

The initial exciton density distribution is supposed to follow the Gaussian distribution $\mathcal{N}(r_0,\sigma^2)$, namely, $n(r-r_0,t=0) = n_0\mathcal{N}(r_0,\sigma^2)$, where n_0 is initial exciton density and σ is its standard deviation. Since the *FWHM* has been determined to be $\sim$220 nm as mentioned before, the remaining fitting parameters to derive $n(r-r_0,t)$ are: R_{eff}, D, and $\tau_{eff,\infty}$, where $\tau_{eff,\infty}$ corresponds to the effective lifetime far from dislocation: we set $\tau_{eff,\infty} = 125$ ps as observed experimentally. As a result, the CL intensity of exciton can be described as $I_{CL}(r-r_0,t) \propto n(r-r_0,t)/\tau_r$, and $\tau_{eff}(r_0)$ can be modelled by fitting $n(r-r_0,t)$, supposing a constant radiative lifetime τ_r. Here, it is important to notice that the two remaining parameters D and R_{eff} are independent and can be tuned almost independently during the fitting procedure. Indeed, the ratio between the effective radius R_{eff} and the *FWHM* of the interaction volume mostly defines the drop observed in the CL intensity at early delays $I_{CL}(t=0)$, since we consider that the dislocation instantaneously acts on the carrier inside the effective dislocation area. On the other hand, the diffusion coefficient D mainly governs the dynamical behavior and hence acts on the effective lifetime $\tau_{eff}(r_0)$ around the dislocation. Such an independence between the two fitting parameters allows us to extract them confidently and provides robustness to our fitting procedure.

As shown in Figs. 3(c) and 3(d), the good agreement between our experimental results and the fits (blue lines) allows us to clearly identify the effective radius of dislocation

$R_{eff} = 95 \pm 3$ nm, the diffusion coefficient $D = 4.5 \pm 0.2$ nm^2/ps, and the effective lifetime $\tau_{eff,\infty} = 125 \pm 3$ ps. Thus, the diffusion length of $D^\circ X_A$ ($L_{Diff} = \sqrt{D\tau_{eff,\infty}}$) can be estimated to be ~24 nm, which indicates that $D^\circ X_A$ are able to diffuse on a short distance by hopping between donor levels.[14,21] Note that the CL intensity at initial delay is defined as $I_{CL}(r_0, t=0) \propto n_0\mathcal{N}/\tau_r$. Considering that no diffusion happens at this moment, the decrease of $I_{CL}(r_0, t=0)$ near the dislocation can be due to either the increase of τ_r or the reduction of n_0. However, the convoluted ~1.3 meV local potential fluctuation of dislocation unlikely changes the wave functions overlap of exciton, which justify why we consider τ_r to be constant over the sample. Therefore, the decrease of $I_{CL}(r_0, t=0)$ near the dislocation should be ascribed to the non-radiative and instantaneous depletion of exciton within R_{eff}. In particular, $R_{eff} = 95 \pm 3$ nm is close to the previously reported value (~50 nm).[11] Even though it is admitted that the core of a pure edge dislocation is at the atomic scale,[22] our results clearly demonstrate that its impact on non-radiative recombination occurs up to the nanoscale, potentially because of the decoration of such dislocation by point defects.[23,24] In addition, in Fig. 3(b), the decay curves at different positions are well reproduced by the fitting equation $I_{CL}(r_0, t) \propto n(r_0, t)/\tau_r$, which further attest our model.

In conclusion, using our picosecond TR-CL, we study the exciton dynamics at 10 K around a single dislocation in bulk epitaxial GaN grown on a free standing GaN substrate at $T = 10$ K. Edge dislocations are identified by observing and simulating the ~1.3 meV dipole-like energy shift, due to the local strain fields induced by such type of dislocation. We determine the effective radius of dislocation $R_{eff} \sim 95$ nm and the diffusion length $L_{diff} \sim 24$ nm of $D^\circ X_A$ by fitting the 1D mappings of CL intensity at early delay time $I_{CL}(r_0, t=0)$ and effective lifetime $\tau_{eff}(r_0)$ around this dislocation, through a 2D exciton diffusion model. Therefore, our results pioneer an innovative way to quantitatively study the influence of dislocation on the efficiency of optoelectronic devices.

The present work was financially supported by the Swiss National Science Foundation under Project Nos. 153620 and 154853 and by the EPFL fellowship program co-funded by Marie Curie (FP7 Grant Agreement No. 291771). We also thank the Attolight Company for the constant improvement of the TR-CL setup.

[1] C. Weisbuch, M. Piccardo, L. Martinelli, J. Iveland, J. Peretti, and J. S. Speck, Phys. Status Solidi A **212**, 899 (2015).
[2] S. J. Rosner, E. C. Carr, M. J. Ludowise, G. Girolami, and H. I. Erikson, Appl. Phys. Lett. **70**, 420 (1997).
[3] S. Nakamura, Science **281**, 956 (1998).
[4] S. Pimputkar, J. S. Speck, S. P. DenBaars, and S. Nakamura, Nat. Photonics **3**, 180 (2009).
[5] J. Cho, E. F. Schubert, and J. K. Kim, Laser Photon. Rev. **7**, 408 (2013).
[6] C. A. Hurni, A. David, M. J. Cich, R. I. Aldaz, B. Ellis, K. Huang, A. Tyagi, R. A. DeLille, M. D. Craven, F. M. Steranka, and M. R. Krames, Appl. Phys. Lett. **106**, 031101 (2015).
[7] R. Liu, A. Bell, F. A. Ponce, C. Q. Chen, J. W. Yang, and M. A. Khan, Appl. Phys. Lett. **86**, 021908 (2005).
[8] X. H. Wu, C. R. Elsass, A. Abare, M. MacK, S. Keller, P. M. Petroff, S. P. Denbaars, J. S. Speck, and S. J. Rosner, Appl. Phys. Lett. **72**, 692 (1998).
[9] G. Pozina, R. Ciechonski, Z. Bi, L. Samuelson, and B. Monemar, Appl. Phys. Lett. **107**, 251106 (2015).
[10] M. Albrecht, L. Lymperakis, and J. Neugebauer, Phys. Rev. B **90**, 241201(R) (2014).
[11] T. Sugahara, H. Sato, M. Hao, Y. Naoi, S. Kurai, S. Tottori, K. Yamashita, K. Nishino, L. T. Romano, and S. Sakai, Jpn. J. Appl. Phys., Part 2 **37**, L398 (1998).
[12] M. Merano, S. Sonderegger, A. Crottini, S. Collin, P. Renucci, E. Pelucchi, A. Malko, M. H. Baier, E. Kapon, B. Deveaud, and J.-D. Ganière, Nature **438**, 479 (2005).
[13] S. Sonderegger, E. Feltin, M. Merano, A. Crottini, J. F. Carlin, R. Sachot, B. Deveaud, N. Grandjean, and J. D. Ganière, Appl. Phys. Lett. **89**, 232109 (2006).
[14] M. Shahmohammadi, J.-D. Ganière, H. Zhang, R. Ciechonski, G. Vescovi, O. Kryliouk, M. Tchernycheva, and G. Jacopin, Nano Lett. **16**, 243 (2016).
[15] T. Onuma, Y. Kagamitani, K. Hazu, T. Ishiguro, T. Fukuda, and S. F. Chichibu, Rev. Sci. Instrum. **83**, 043905 (2012).
[16] D. Gogova, A. Kasic, H. Larsson, B. Pécz, R. Yakimova, B. Magnusson, B. Monemar, F. Tuomisto, K. Saarinen, C. Miskys, M. Stutzmann, C. Bundesmann, and M. Schubert, Jpn. J. Appl. Phys., Part 1 **43**, 1264 (2004).
[17] H. Lu, X. A. Cao, S. F. LeBoeuf, H. C. Hong, E. B. Kaminsky, and S. D. Arthur, J. Cryst. Growth **291**, 82 (2006).
[18] N. Gmeinwieser, P. Gottfriedsen, U. T. Schwarz, W. Wegscheider, R. Clos, A. Krtschil, A. Krost, A. Weimar, G. Brüderl, A. Lell, and V. Haürle, J. Appl. Phys. **98**, 116102 (2005).
[19] N. Gmeinwieser and U. T. Schwarz, Phys. Rev. B **75**, 245213 (2007).
[20] W. R. Harding, I. D. Blenkinsop, and D. R. Wight, Electron. Lett. **12**, 503 (1976).
[21] G. Jacopin, M. Shahmohammadi, J.-D. Ganière, and B. Deveaud, Appl. Phys. Lett. **104**, 042109 (2014).
[22] S. L. Rhode, M. K. Horton, W. Y. Fu, S.-L. Sahonta, M. J. Kappers, T. J. Pennycook, C. J. Humphreys, R. O. Dusane, and M. A. Moram, Appl. Phys. Lett. **107**, 243104 (2015).
[23] A. Pinos, S. Marcinkevičius, M. Usman, and A. Hallén, Appl. Phys. Lett. **95**, 112108 (2009).
[24] A. Krtschil, A. Dadgar, and A. Krost, J. Cryst. Growth **248**, 542 (2003).